



Research Article

# Comprehensive performance, combustion, emission, and vibration parameters assessment of diesel engine fuelled with a hybrid of niger seed oil biodiesel and hydrogen: response surface methodology approach

Jai Kumar Sagari<sup>1</sup> · Bhatti Sukhvinder Kaur<sup>2</sup> · Srinivas Vadapalli<sup>1</sup> · Vamsi Teja Dadi<sup>1</sup> · Sai Susmitha Guddanti<sup>1</sup> · Santosh Kumar Lakkoju<sup>3</sup>

Received: 28 October 2019 / Accepted: 5 August 2020 / Published online: 13 August 2020  
© Springer Nature Switzerland AG 2020

## Abstract

The present investigation centered on the application of response surface methodology to assess the engine operating parameters namely performance, combustion, emission, and vibration characteristics of variable compression ratio direct injection single-cylinder diesel engine operating with Niger seed oil methyl ester blend and hydrogen in dual fuel mode. Response surface models were developed using the experimental data of input and output variables. The fuel blend, load, compression ratio, and hydrogen flow rate were considered as input responses while the brake thermal efficiency, brake specific fuel consumption, cylinder pressure and net heat release rate, carbon monoxide (CO), unburnt hydrocarbon, Nitrogen oxides (NO<sub>x</sub>), smoke opacity, and RMS velocity respectively were considered as the output responses. The input conditions altered were: loads of 29.43 N (3 kgf), 58.86 N (6 kgf), 88.29 N (9 kgf), and 117.72 N (12 kgf), compression ratios of 16, 17.5, and 18.5, and the hydrogen flow rates of 5 lpm, 10 lpm, and 15 lpm. The output information of the test was assessed using response surface methodology (RSM) and the polynomial model (second-request) was created. The experimental values were in good match with RSM predicted values and maintained an R<sup>2</sup> value of more than 0.95 for all the test run combinations. Further, all the test points sustained comparatively within the 10% maximum deviation.

**Keywords** Brake thermal efficiency · Compression ratio · Smoke opacity · Hydrogen · Cylinder pressure

## Abbreviations

CR	Compression ratio	CI	Compression ignition
FB	Fuel blend	ASTM	American standards for testing materials
HFR	Hydrogen flow rate (lpm)	ADC	Analog to digital converter
BTE	Brake thermal efficiency (%)	lpm	Liter per minute
BSFC	Brake specific fuel consumption (kg/kWhr)	CP	Cylinder pressure (bar)
NSOME	Niger seed oil methyl ester	NHRR	Net heat release rate (J/deg.)
B20	20% NSOME in diesel	$\frac{\delta q}{\delta \theta}$	Net heat release rate (J/deg.)
CO	Carbon monoxide (%)	$\frac{\delta q_{Heat}}{\delta \theta}$	Heat transfer rate combustion chamber wall (J/deg.)
UHC	Unburnt hydrocarbon (ppm)	$\frac{\delta V}{\delta \theta}$	Volume change with crank angle (m <sup>3</sup> /deg.)
NOx	Nitrogen oxides (ppm)	$\frac{\delta p}{\delta \theta}$	Pressure change with crank angle (bar/deg.)

✉ Jai Kumar Sagari, sagari.jaikumar1@gmail.com | <sup>1</sup>Department of Mechanical Engineering, GITAM University, Visakhapatnam, India. <sup>2</sup>Department of Mechanical Engineering, Andhra University, Visakhapatnam, India. <sup>3</sup>Department of Physics, Anil Neerukonda Institute of Technology and Sciences, Visakhapatnam, India.



SN Applied Sciences (2020) 2:1508 | <https://doi.org/10.1007/s42452-020-03304-x>

$\gamma$	Specific heats ratio
$p$	Cylinder pressure (Instantaneous)
$c_p$	Specific heat at constant pressure (J/Kg-K)
$c_v$	Specific heat at constant volume (J/Kg-K)
$V_{RMS}$	RMS velocity (m/s)
tfc	Total fuel consumption (Kg/hr)
CV	Calorific value (MJ/kg)
bp	Brake power (kW)
$\Delta BTE$	Uncertainty in BTE
$\Delta BSFC$	Uncertainty in BSFC
$\Delta CO$	Uncertainty in CO
$\Delta UHC$	Uncertainty in UHC
$\Delta NO_x$	Uncertainty in $NO_x$
$\Delta Smoke$	Uncertainty in smoke opacity

## 1 Introduction

Compared to the last few decades, the demand for energy has increased exponentially. Moreover, somewhat the oil reserves have been depleting continuously which leads to its increase in price. Therefore, an alternate fuel source plays a significant role in the development of energy demand, economic improvement of the nation, and reduction of pollution [1, 2]. Vegetable oils are regarded as a potential substitute intended for conventional diesel because it has equivalent properties with standard diesel [3–5]. Several investigations have been carried out with biodiesels derived from different raw vegetable oils and used in the application of diesel engines to assess the performance, combustion, and exhaust emission characteristics [4, 5]. Senthur et al. [6] reported that the brake specific fuel consumption of used cooking oil methyl ester was increased due to lower heating value and also found that there is a significant reduction in carbon monoxide, unburnt hydrocarbon, and nitrogen oxides emissions has increased slightly. Sal methyl ester was used in the CI engine by Harveer et al. [7] to assess the performance and emissions studies. They revealed that the CO, UHC, and smoke were observed lower excluding the  $NO_x$ . Ahmet et al. [8] explored the performance and emission analysis of mustard oil biodiesel blends. They concluded that an increase in BTE (6.8%) and a drop in BSFC (4.8%) were noticed with B10. Besides, the CO and smoke emissions were dropped down except for  $NO_x$ . The foremost complexity with the use of biodiesel in a diesel engine is an inferior BTE and irrelevant smoke emissions. These difficulties can be resolved by introducing gaseous fuels in conjunction with primary fuel. Hydrogen is a carbon-free fuel among all the gaseous fuels which reducing the emissions of CO, UHC, and particulate matter apart from  $NO_x$ . Hydrogen enrichment could decrease the heterogeneity of diesel or biodiesel fuel and result in superior premixing with

air to make the combustible mixture uniform [9]. Mohanad et al. [10] explored an improved performance and the emission reduction (apart from  $NO_x$ ) of Rapeseed methyl ester blend (B20) and hydrogen fueled diesel engine. Rahman et al. [11] investigated the performance and emission parameters of the CI engine in dual fuel operation using biodiesel blend B40 and hydrogen at the flow rate of 4 lpm. They reported that the BTE was improved by 21.9% compared to standard diesel fuel. Further, UHC and smoke opacity emissions reduced by 63.3% and 22% individually. Jaikumar et al. [12] conducted an experiment to assess diesel engine operating parameters namely performance, combustion, and emission characteristics using Niger seed oil biodiesel and hydrogen in dual fuel mode by altering compression ratios. They concluded that the BTE, CP, NHRR, RoPR, and  $NO_x$  were improved while the BSFC, CO, UHC, and smoke opacity were reduced with hydrogen enrichment. The multi-objective optimization techniques in the application of CI engine with different operating parameters are limited. Response surface methodology (RSM) is one of the best contemporary optimization techniques for experimental outcomes [13]. Rao et al. [14] performed parametric optimization using response surface methodology (RSM) and Grey relational analysis (GRA) optimization technique for the assessment of CI engine operating characteristics by fueling Mahua biodiesel and methanol blends. They reported that the experimental results are approximately similar to validated results in terms of the desirability approach. The best outcome was specified at a load of 20 kg and B100 + 3% methanol. Bharadwaz et al. [15] perform an optimization study through RSM to assess the process parameters of CI engine fuelled with biodiesel-ethanol blends by varying different compression ratios. They concluded that RSM is a useful method to optimize the CI engine process parameters. Molina et al. [16] conducted an optimization study using response surface methodology technique to assess the performance and emission parameters of CI engine. They concluded that the average errors of specific fuel consumption and  $NO_x$  were 6% and 2%, respectively. Jaikumar et al. [17] carried out an experimental investigation on the VCR diesel engine to assess the vibration and noise parameters by fuelling with Niger seed oil biodiesel and hydrogen in dual mode. They reported that the RMS velocity (vibration) and RMS noise of B20 were observed less compared to other blends. Besides, the decrease in vibration and noise was noticed upon the addition of hydrogen to B20. However, the engine vibration and noise were increased at higher compression ratios.

Based on the past research occurrence of various investigators, the studies connected to RSM application for the assessment of VCR diesel engine process parameters are very limited. A few studies have been performed on

performance and emission parameters apart from combustion and vibration characteristics. Hence, the present investigation is focused on the application of RSM in the prediction of performance, combustion, emission, and vibration process parameters namely of VCR diesel engine operating with Niger seed oil biodiesel and hydrogen which is a fairly novel endeavor.

## 2 Materials and methodology

NSOME was used in the current investigation which was produced through the transesterification process. The physicochemical properties of NSOME were tested under the ASTM standards. Table 1 presents the physicochemical properties of NSOME. Further, two test fuels were used in this study namely diesel and B20. The B20 was prepared by blending the NSOME (20% by volume) with standard diesel (80% by volume). In this experimentation, a single-cylinder, water-cooled, variable compression ratio, and a four-stroke engine is used for analysis. The schematic of the test rig is depicted in Fig. 1 and the engine test setup specifications presented in Table 2. VCR engine is linked with two separate tanks which are used intended for diesel and biodiesel respectively. The tanks are connected to a fuel flow sensor demonstrating the fuel consumption throughout the experiment. Further, the inlet engine section is equipped with an air-box along with the airflow sensor, and also the hydrogen cylinder was connected through the mass flow meter to inlet of the engine while on the exhaust side of the engine, a 5-gas analyzer and smoke meter were linked to measuring the emissions. The engine is also coupled with an eddy current dynamometer. Finally, a Polytec Doppler Vibrometer-100 (PDV-100) was linked near the engine to assess the vibration intensity through a laser beam. Specifications of LDV were presented in Table 3. The details of instruments used and their accuracy are depicted in Table 4.

Before the preparatory experiment, the engine test rig is allowed for read-through power supply, level of lubricating oil, and the cold water supply. Subsequently, the test fuels were used on a single-cylinder, 4-stroke VCR diesel engine at a constant speed of 1500 rpm. The compression

ratio was varied like 16, 17.5, and 18.5 respectively while the engine loads were 29.43 N (3 kgf), 58.86 N (6 kgf), 88.29 N (9 kgf), and 117.72 N (12 kgf). Further, the mix of B20 was enriched with hydrogen at the flow rates of 5 lpm, 10 lpm, and 15 lpm individually. A similar procedure was carried out with the aforementioned loads and compression ratios for hydrogen-enriched B20. The readings were taken after the stabilization of the engine. The performance parameters were estimated considering the rundown time in the burette for 10 cubic centimeters (volume). The performance parameters were calculated using the following Eqs. (1)–(3).

$$BTE = \frac{bp}{(tfc \times CV)} \quad (1)$$

$$BTE = \frac{bp}{(tfc \times CV) + ((H_2 \text{ consumed} / \text{kg}) \times CV)} \quad (2)$$

$$BSFC = \frac{tfc}{bp} \quad (3)$$

where BTE, bp, tfc, CV,  $H_2$ , CV, and BSFC are brake thermal efficiency, brake power, total fuel consumption, calorific value, hydrogen, and brake specific fuel consumption respectively.

The combustion characteristics were recorded using “IC Engine soft” software. The NHRR was calculated according to the first law of thermodynamics with the help of Eq. (4).

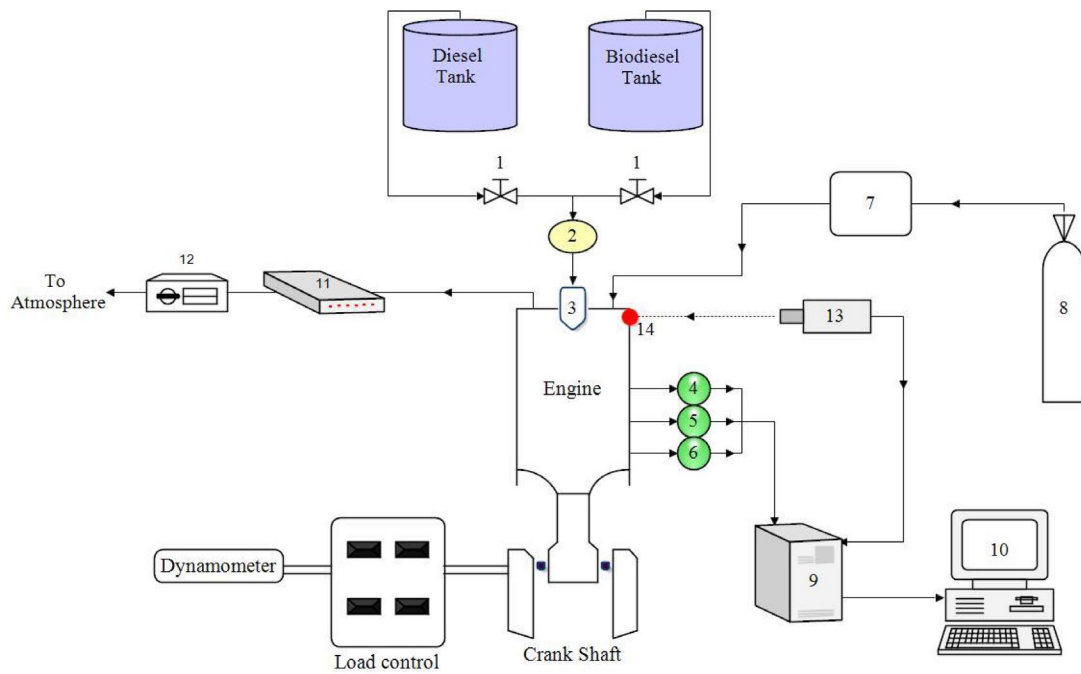
$$\frac{\delta q}{\delta \theta} = \frac{1}{\gamma - 1} V \frac{\delta p}{\delta \theta} + \frac{\gamma}{\gamma - 1} p \frac{\delta V}{\delta \theta} + \frac{\delta q_{Heat}}{\delta \theta} \quad (4)$$

where  $\gamma = \frac{c_p}{c_v}$ .

Further, the emission (CO, UHC, NO<sub>x</sub>, and smoke) parameters were estimated using MARS 5 gas analyzer and MARS smoke meters respectively. Finally, the vibration (RMS velocity) signals were captured by a dual-channel FFT analyzer and USB based vibrosoft-20 software. Moreover, the vibration signals were recorded at a fixed point on the engine head by allowing the laser beam, and these captured signals were mapped. The RMS velocity is calculated with the aid of Eq. (5).

**Table 1** Physicochemical properties

Fuel property	Method	ASTM	NSOME
Relative density at 15 °C (kg/m <sup>3</sup> )	ASTM D-1298	860–900	888.6
Kinematic viscosity at 40 °C (Centi Stokes)	ASTM D-445	2.5–6	4.14
Heating value (MJ/kg)	ASTM D -4809	42	41.25
Cetane number	ASTM D-976	47 (min.)	59
Copper corrosion	ASTM D-130	1 (max)	1a
Cloud point (°C)	ASTM D-97	6 (max.)	3
Flashpoint (°C)	ASTM D-92	130 (min.)	157



- 1. Control valves
- 2. Fuel flow sensor
- 3. Fuel injector
- 4. Pressure sensor
- 5. Crankangle sensor
- 6. Temperature sensor
- 7. Hydrogen flow meter
- 8. Hydrogen cylinder
- 9. DAQ
- 10. computer
- 11. 5-gas analyzer
- 12. Smoke meter
- 13. LDV
- 14. Laser beam

Fig. 1 Schematic diagram of experimental setup

Table 2 Engine specifications

Parameter	Description
Type	TAF-1, VCR multi fuel, single cylinder, water-cooled, 4 stroke, direct injection engine
Ignition	Compression ignition
Stroke/Bore	110 mm/87.5 mm
Rated BP (Brake power)	3.5 kW with diesel, 4.5 kW with petrol
Engine speed	1500 rpm
Engine load	3 kgf, 6 kgf, 9 kgf, and 12 kgf
Injection point	30° Before TDC
CRs	16,17.5,18.5

Table 3 LDV specifications

Parameter	Description
Type	PDV-100 Portable Digital Vibrometer
model of Impact hammer	086C03
Software used	USB based, dual channel Vibrosoft-20

$$v_{RMS} = \left[ \frac{1}{n} \sum_{i=1}^n v^2(t_i) \right]^{\frac{1}{2}} \tag{5}$$

The total uncertainty of measured variables was calculated with the aid of Eq. (6).

$$U_R = \sqrt{\left\{ \left( \frac{\partial F}{\partial X} u_1 \right)^2 + \left( \frac{\partial F}{\partial X} u_2 \right)^2 + \left( \frac{\partial F}{\partial X} u_3 \right)^2 + \dots + \left( \frac{\partial F}{\partial N} u_N \right)^2 \right\}} \tag{6}$$

where  $U_R$  is the uncertainty in total,  $F$  is the uncertainty function;  $u_1, u_2, u_3,$  and  $u_N$  are the uncertainties of individual variables.

**Table 4** Accuracy and measurements

Measurement constraint	Accuracy	Limit
Load sensor	±0.2 kg	0–50 kg
speed sensor	± 25 rpm	1200–1800 rpm
Temperature sensor	± 1%	0–100 °C
Crank angle sensor	±0.1%	resolution of 1°
CO	±0.001%	0–99.9%
UHC	± 2 ppm	0–15,000 ppm
NOx	± 1 ppm	0–5000 ppm
Smoke	±0.1%	0–99.9%

$$U_R = \sqrt{\{(\Delta BTE)^2 + (\Delta BSFC)^2 + (\Delta CO)^2 + (\Delta UHC)^2 + (\Delta NO_x)^2 + (\Delta Smoke)^2\}} \tag{7}$$

$$U_R = \sqrt{\{(1.4)^2 + (1.3)^2 + (0.7)^2 + (0.6)^2 + (0.8)^2 + (0.6)^2\}} \tag{8}$$

The total uncertainty is ± 2.32%

### 3 Response surface methodologies (RSM)

Response surface methodology is the numerical technique to model and analyzes diverse problems during optimization of process parameters. The desirability approach is used in multi-response problems to hold the benefit of accessibility and flexibility in response adjustment [18]. The present study intends to model and predict the experimental process output responses using the RSM technique. The output experimental data was assessed by developing a second-order polynomial model and regression. The developed second-order polynomial equation was significant mathematically, and hence it sets for a relationship between input and output responses. Finally, the predicted output responses were produced by response surface plots using fit models.

The experiments were planned with their selected level as fuel blend, engine load, compression ratio, and hydrogen flow rate for input responses with one set of experiments. The output responses considered such as BTE and BSFC intended for performance characteristics, CP and NHRR used for combustion characteristics, CO, UHC, NOx, and smoke opacity for the emission characteristics, and RMS velocity for vibration characteristics. The design used in this analysis was Box-Behnken design. This model

analyses the result of each independent operating condition of the yield. The following quadratic Eq. (9) was used in this model.

$$Y = \beta_0 + \sum_{j=1}^k \beta_j X_j + \sum_{j=1}^k \beta_{jj} X_j^2 + \sum_{j=1}^k \sum_{i=j+1}^k \beta_{ij} X_i X_j \tag{9}$$

$\beta_0, \beta_j, \beta_{jj}$ , and  $\beta_{ij}$  are the constant, the coefficient of linear term, the coefficient of quadratic term, and the coefficient of cross term, correspondingly.  $i$  and  $j$  are the linear and quadratic factors,  $k$  is the number of factors studied and optimized.  $X_j$  and  $X_i$  are independent operating variables.  $Y$  is the output response. The design matrix was generated in “Design Expert” containing 60 runs. After the experiment, the model was analyzed using analysis of variance (ANOVA).

## 4 Results and discussions

### 4.1 Performance parameters

#### 4.1.1 Brake thermal efficiency (BTE)

Figure 2a, b portray the response surfaces of BTE against load, compression ratio, and hydrogen flow rate while Fig. 2c, d depict the comparison in experimental and RSM predicted output responses. It can be distinguished from Fig. 2a, b that the BTE was directly proportional to the load, compression ratio, and hydrogen flow rate. The BTE of hydrogen-enriched B20 was noticed higher than normal diesel and B20. Because the hydrogen addition could develop extra power due to the superior mixing of air and fuel. BTE at higher loads superior on account elevated mechanical efficiency. Further, the friction losses from the combustion chamber wall and also the heat loss could reduce with enrichment of hydrogen and consequently higher the BTE. Also, BTE was depicted higher at a superior compression ratio due to enhanced compression temperature which elevates the combustion efficiency [18, 19]. Maximum BTE was noticed as 28.86% at a combination of CR 18.5, HFR 15 lpm, and 12 kgf load condition. It can also be noticed that from Fig. 2c, d that the correlation between experimental and RMS predicted BTE values are accurate with very little error. A similar repetition was attained almost at all the test run combinations. The correlation coefficient  $R^2$  was attained as 0.99 which was a better fit.

$$\begin{aligned} \text{BTE}(\%) = & (-0.3390 \times FB) + (0.6446 \times CR) + (6.78 \times Load) + (0.6685 \times HFR) + (0.0284 \times FB \times CR) \\ & + (0.0151 \times FB \times Load) + (0.0000 \times FB \times HFR) + (0.0276 \times CR \times Load) + (0.0872 \times CR \times HFR) \\ & + (0.2644 \times Load \times HFR) + (0.0000 \times FB^2) - (0.0907 \times CR^2) - (3.43 \times Load^2) - (0.1568 \times HFR^2) \end{aligned} \tag{10}$$

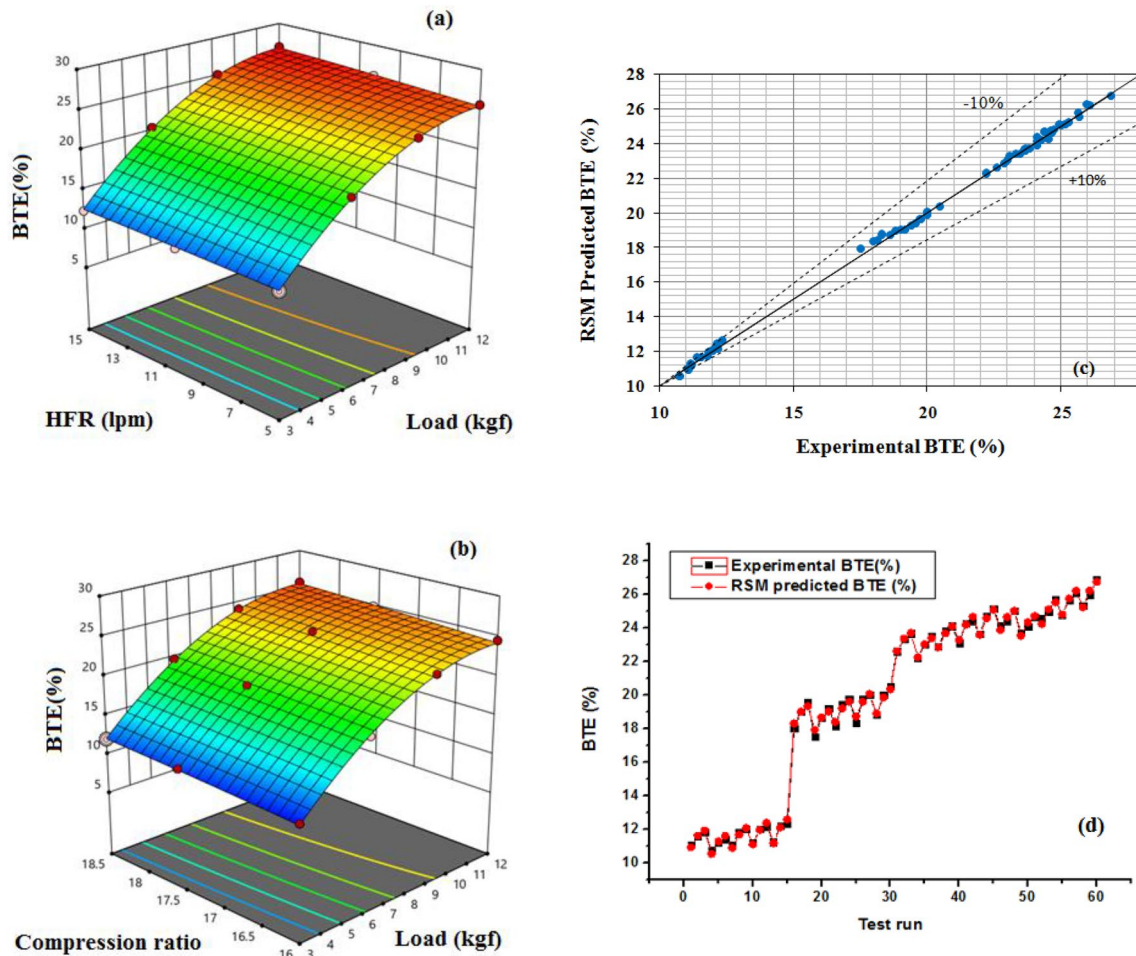


Fig. 2 **a, b** Response surfaces of BTE. **c** Experimental against RSM predicted BTE. **d** BTE at different test runs

### 4.1.2 Brake specific fuel consumption (BSFC)

Figure 3a, b show the variation in BTE as response surfaces adjacent to compression ratio, load, and hydrogen flow rate whereas the experimental and RSM predicted values were depicted in Fig. 3c, d. It can be seen that the BSFC was dropped at upper load conditions (Fig. 3a, b) intended for all the experiment fuels. This was due to air entrainment, enhanced diffusion of fuel, and faster penetration. Upon hydrogen enrichment, the drop-down in BSFC was seen due to the superior atomization of fuel. Further, BSFC was reduced at a higher compression ratio due to advanced atomization [18, 19]. It can be accomplished that the BSFC was decreased with an increase in compression ratio, hydrogen mass flow rate,

and load. At CR 18.5, HFR 15 lpm, and full load (12 kgf) load condition, the minimum BSFC was attained as 0.30495 kg/kW hr. The observations made from the Fig. 3c, d that the relationship connecting to experimental and RMS predicted BSFC was perfect with a lesser inaccuracy. The analogous recurrence was attained almost at all the test run combinations.  $R^2$  was obtained as 0.989 indicating the superior correlation of experimental and predicted results.

$$\begin{aligned}
 \text{BSFC}(kg/kWhr) = & 0.3840 + (0.0118 \times FB) - (0.0194 \times CR) \\
 & - (0.1980 \times Load) - (0.0201 \times HFR) \\
 & - (0.0002 \times FB \times CR) - (0.0024 \times FB \times Load) \\
 & + (0.0000 \times FB \times HFR) + (0.0101 \times CR \times Load) \\
 & + (0.0001 \times CR \times HFR) + (0.0005 \times Load \times HFR) \\
 & + (0.0000 \times FB^2) - (0.0021 \times CR^2) \\
 & + (0.1557 \times Load^2) + (0.0088 \times HFR^2)
 \end{aligned}
 \tag{11}$$

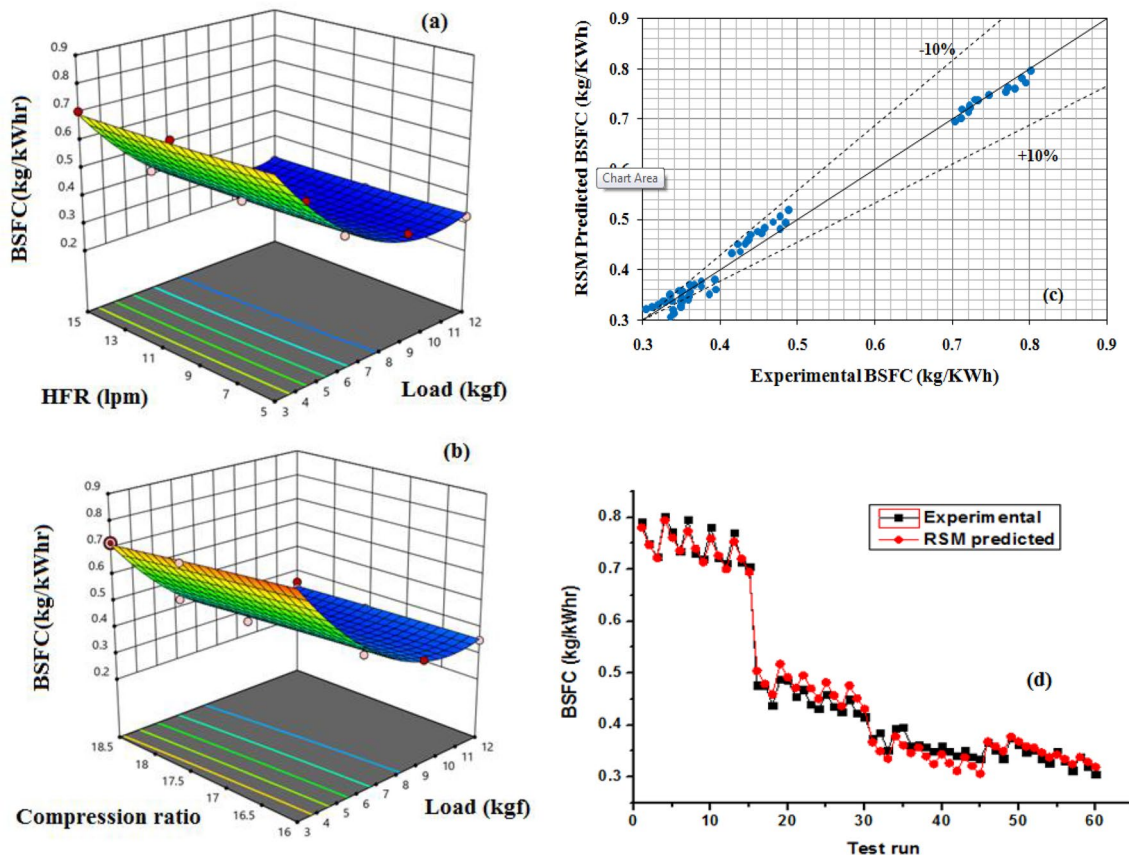


Fig. 3 a, b Response surfaces of BSFC c Experimental against RSM predicted BSFC d BSFC at different test runs

## 4.2 Performance parameters

### 4.2.1 Cylinder pressure (CP)

The response surface disparity in CP regarding input parameters was portrayed in Fig. 4a, b while the experimental and predicted CP values were depicted in Fig. 4 c, d. It was noticed from the Fig. 4a, b was that the peak CP was improved at a higher compression ratio and higher load. The reason was due to rapid flame propagation which was on account of higher in-cylinder pressure and temperature at higher compression ratios [12, 21]. Further, an increase in the hydrogen flow rate was noticed superior CP irrespective of loads and compression ratios. The reason for this extreme rise in CP was due to a large amount of fuel burnt in the premixed stage of combustion. Thus, the turbulence could be created as a result of the superior

rate of diffusion [20] and more quantity of hydrogen accumulated in B20 and therefore the CP increased further. The maximum CP was reached to 62.88 bar at CR 18.5, HFR 15 lpm, and at a full load (12 kgf). The perfect correlation with minimum factual error was attained for experimental and RMS predicted CP. The comparable recurrence was achieved intended for all test runs. The correlation coefficient ( $R^2$ ) was acquired as 0.956 which signifying the better relationship between experimental predicted outputs.

$$\begin{aligned}
 CP(\text{bar}) = & 53.17 + (0.2520 \times FB) + (2.88 \times CR) + (4.06 \times Load) \\
 & + (2.35 \times HFR) + (0.4986 \times FB \times CR) \\
 & + (0.4784 \times FB \times Load) + (0.0000 \times FB \times HFR) \\
 & + (0.3353 \times CR \times Load) - (0.8516 \times CR \times HFR) \\
 & - (0.6763 \times Load \times HFR) + (0.0000 \times FB^2) \\
 & + (1.55 \times CR^2) - (1.33 \times Load^2) + (0.0200 \times HFR^2)
 \end{aligned} \tag{12}$$

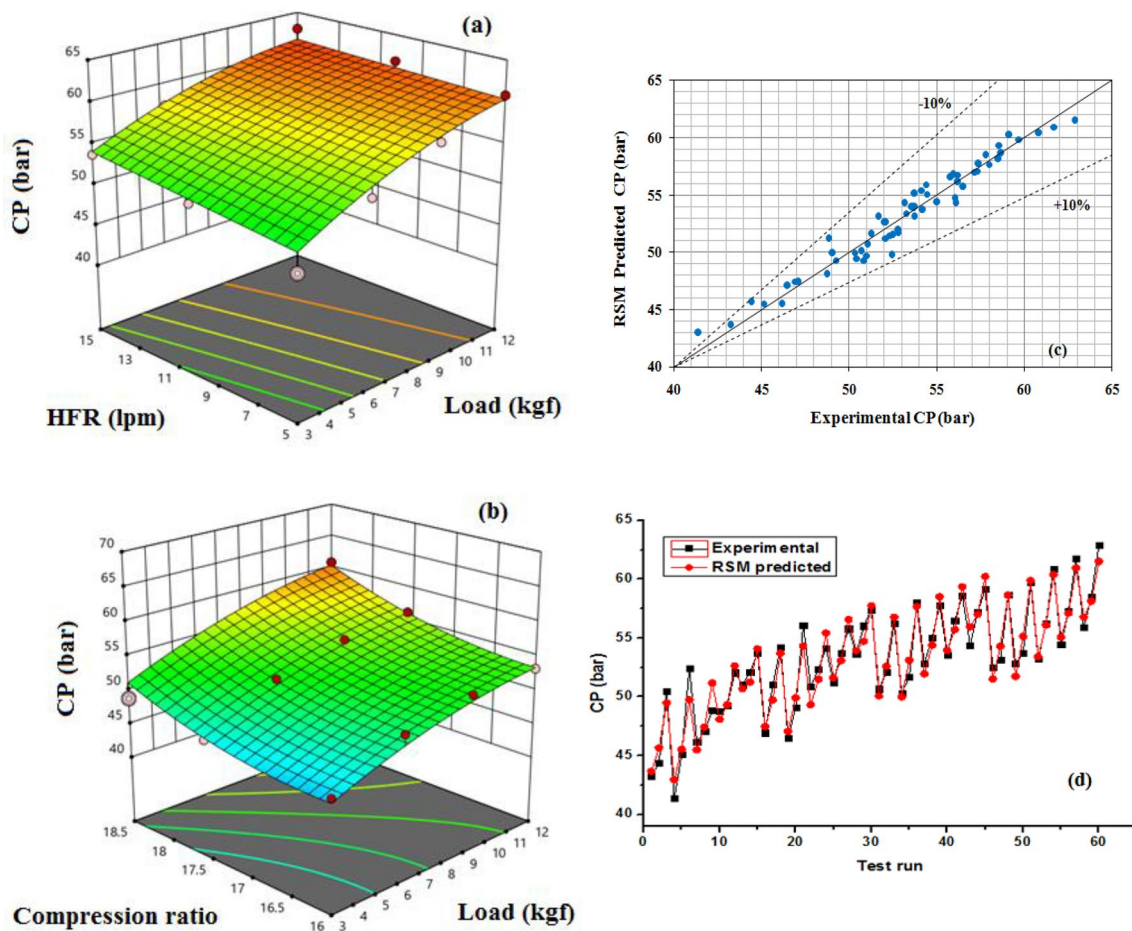


**Fig.4** a, b Response surfaces of CP c Experimental against RSM predicted CP d CP at different test runs

#### 4.2.2 Net heat release rate (NHRR)

Figure 5a, b show the change in NHRR with compression ratio, load, and hydrogen flow rate, while the experimental and prediction result of NHRR was portrayed in Fig. 5c, d. As observed, the NHRR was increased with an increase in the compression ratio. This was mainly on account of enhanced in-cylinder pressure and temperature which lead to the combustion dominance [12]. Also, the NHRR was observed superior with hydrogen enrichment. Increase in hydrogen flow rate, the NHRR was also higher. This could be demonstrated by the occurrence of NHRR in three stages. During the initial stage, the occurrence of premixed combustion intended for normal diesel and biodiesel fairly in advance compared to hydrogen fuel. Consequently, the entrainment of hydrogen and air in diesel and biodiesel could be a small extent. In the subsequent stage, the premixed combustion of hydrogen

dominates combustion with conventional diesel and biodiesel at the fuel spray zone. The concluding period implies diffusion combustion intended for all three fuels. Throughout this period, the flame propagates rapidly towards hydrogen fuel from the spray zone and hence it augments the laminar flame speed right through the combustion chamber, thus liberating a great quantity of heat [10, 12]. It can also be noted that at higher loads the release rate of heat was high due to better mixing of air and fuel. The maximum peak NHRR was noticed as 68.81 J/degree at CR 18.5, HFR 15 lpm, and at full load (12 kgf). The observations noticed from Fig. 5c, d that the experimental and RSM predicted NHRR correlation was flawless. The comparable re-emergence was noticed with all test runs. The  $R^2$  value was noticed as 0.976 suggesting a good correlation of experimental and RSM predicted results.



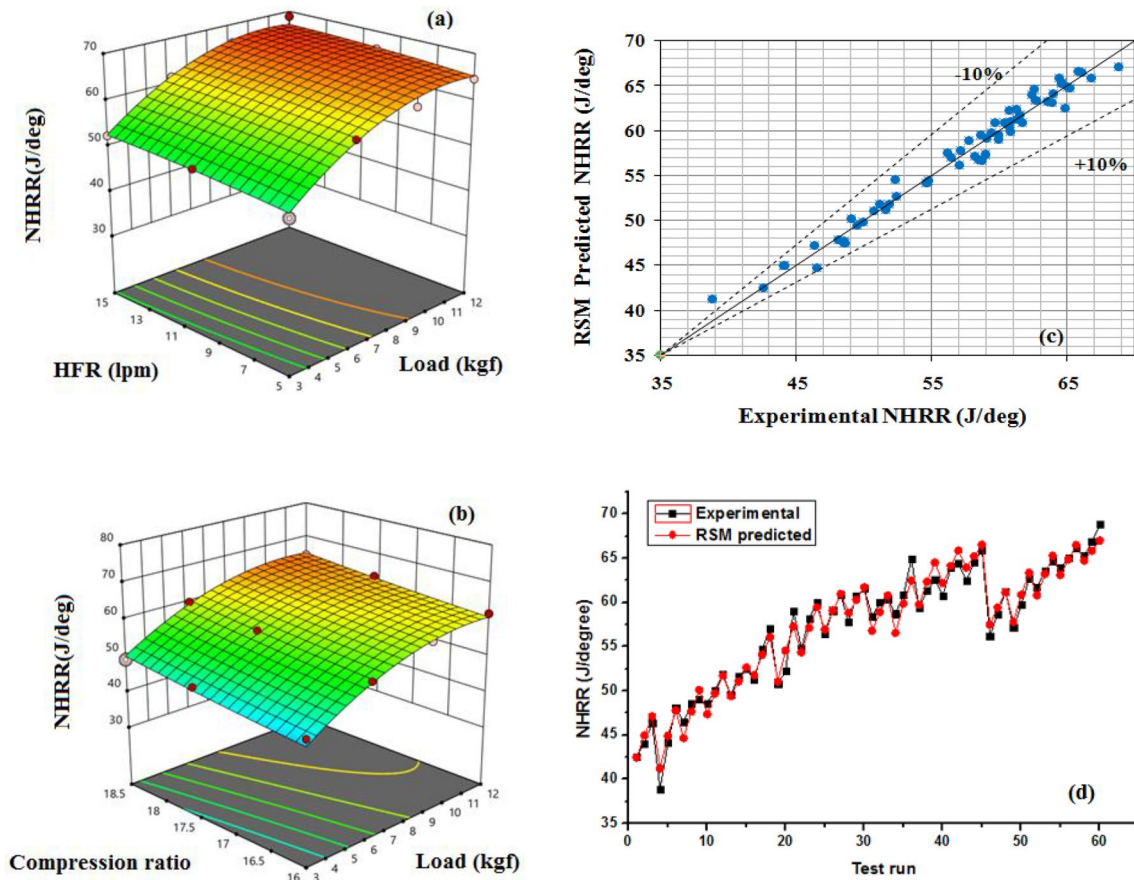


Fig.5 a, b Response surfaces of NHRR c Experimental against RSM predicted NHRR d NHRR at different test runs

$$\begin{aligned}
 \text{NHRR}(J/\text{deg}) = & 60.83 + (0.4990 \times FB) + (2.20 \times CR) \\
 & + (7.73 \times \text{Load}) + (2.95 \times \text{HFR}) \\
 & + (0.9480 \times FB \times CR) + (0.7549 \times FB \times \text{Load}) \\
 & + (0.0000 \times FB \times \text{HFR}) - (0.2444 \times CR \times \text{Load}) \\
 & - (0.8290 \times CR \times \text{HFR}) - (0.3023 \times \text{Load} \times \text{HFR}) \\
 & + (0.0000 \times FB^2) + (0.2738 \times CR^2) \\
 & - (4.85 \times \text{Load}^2) - (0.7794 \times \text{HFR}^2)
 \end{aligned}
 \tag{13}$$

### 4.3 Emission parameters

#### 4.3.1 Carbon monoxide (CO)

Figure 6a, b depict the disparity in response surface of CO adjacent to compression ratio, load, and hydrogen flow rate while the experimental CO and RSM predicted CO was depicted in Fig. 6c, d. It can be noticed from the Fig. 6a, b that the CO emission was decreased with

enrichment of hydrogen due to reduced equivalent ratio and elevated combustion [22]. Further, at higher compression ratios the CO was noticed lower on account of superior combustion efficiency [12]. The momentous augment in CO was also perceived at higher loads. The least CO was obtained as 0.001% at CR 18.5, HFR of 15 lpm, and at a load condition of 3 kgf. The observations noticed from the Fig. 6c, d that the experimental and RMS predicted CO correlation was flawless. A similar repetition was noticed intended for all tests. R<sup>2</sup> value was noticed as 0.969 signifying fine relationships between experimental and RSM predicted CO.

$$\begin{aligned}
 \text{CO}(\%) = & 0.0080 - (0.0385 \times FB) - (0.0031 \times CR) \\
 & + (0.0127 \times \text{Load}) - (0.0069 \times \text{HFR}) \\
 & + (0.0034 \times FB \times CR) - (0.0247 \times FB \times \text{Load}) \\
 & + (0.0000 \times FB \times \text{HFR}) - (0.0027 \times CR \times \text{Load}) \\
 & + (0.0008 \times CR \times \text{HFR}) - (0.0098 \times \text{Load} \times \text{HFR}) \\
 & + (0.0000 \times FB^2) + (0.0001 \times CR^2) \\
 & + (0.0060 \times \text{Load}^2) + (0.0044 \times \text{HFR}^2)
 \end{aligned}
 \tag{14}$$

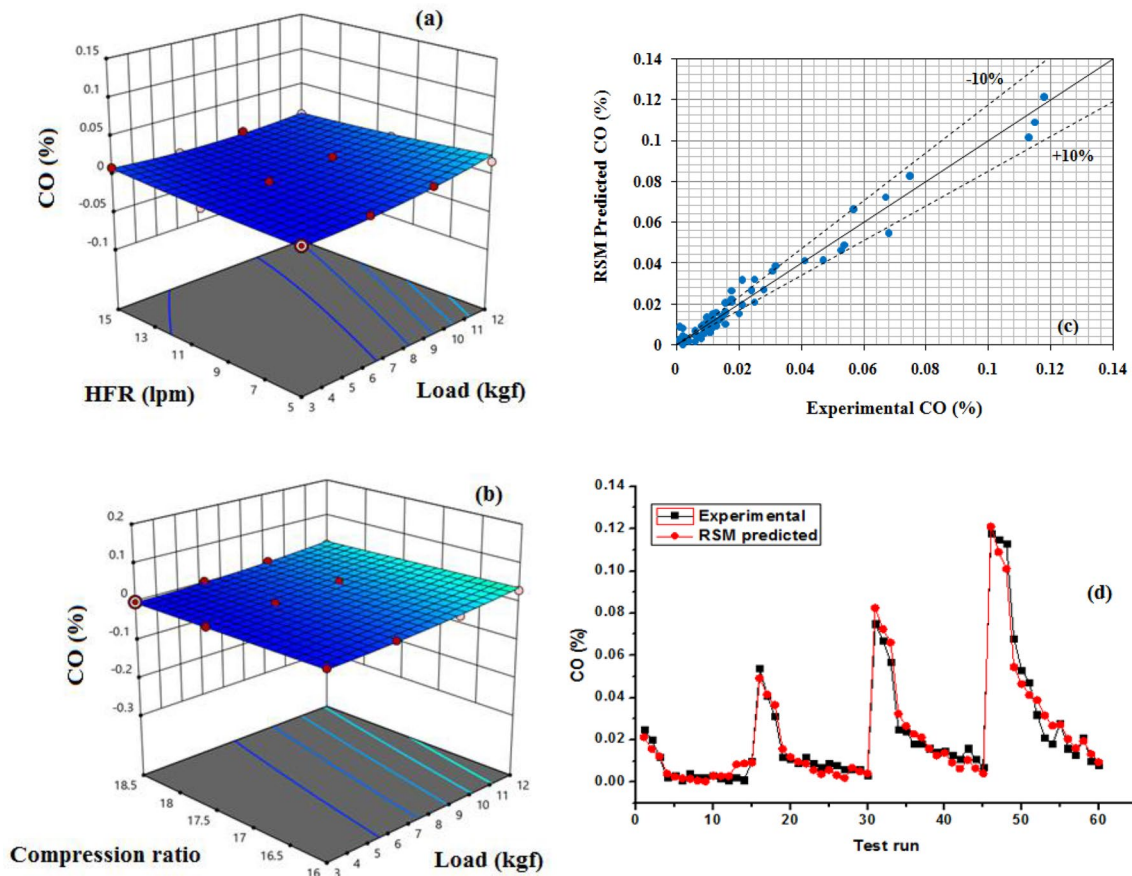


**Fig.6** a, b Response surfaces of CO c Experimental against RSM predicted CO d CO at different test runs

### 4.3.2 Unburnt hydrocarbons (UHC)

Figure 7a, b portray the change in UHC against compression ratio, load, and hydrogen flow rate while the experimental UHC and predicted UHC was represented in Fig. 7c, d. From Fig. 7a, b, the UHC emissions were noticed lower as the hydrogen flow rate increased owing to an increased ratio of hydrogen and carbon. Since the hydrogen has negligible carbon content and thus UHC emissions were reduced. Further, the UHC emissions reduced towards upper compression ratios given superior combustion efficacy [12, 23]. The significant increase in UHC was also observed towards higher load conditions. Lower UHC was noticed as 25 ppm at CR 18.5, 3 kgf load condition, and at an HFR of 15 lpm. From Fig. 7c, d, the experimental and RMS predicted UHC association was perfect. Alike recurrence was discerned with all test run conditions. The  $R^2$  value was perceived as 0.97.

$$\begin{aligned}
 \text{UHC(ppm)} = & 45.54 - (28.84 \times FB) - (8.22 \times CR) + (12.33 \times Load) - (18.81 \times HFR) + (3.29 \times FB \times CR) \\
 & - (9.88 \times FB \times Load) + (0.0000 \times FB \times HFR) - (2.73 \times CR \times Load) + (2.00 \times CR \times HFR) \\
 & - (8.86 \times Load \times HFR) + (0.0000 \times FB^2) - (0.5521 \times CR^2) + (6.07 \times Load^2) + (5.72 \times HFR^2)
 \end{aligned} \tag{15}$$

### 4.3.3 Nitrogen Oxides (NO<sub>x</sub>)

Figure 8a, b represent the NO<sub>x</sub> emission against compression ratio, load, and hydrogen flow rate while the Fig. 8c, d show the experimental and RSM predicted NO<sub>x</sub>. As observed, the NO<sub>x</sub> was enhanced at higher hydrogen flow rates and higher compression ratios. The reason behind this increase was on account of an increase in in-cylinder temperature and pressure which was due to higher oxygen availability and higher speed of combustion [12, 19]. The momentous rise in NO<sub>x</sub> was observed at upper loads. The maximum NO<sub>x</sub> was specified as 1209 ppm at CR 18.5, 12 kgf (full) load, and HFR of 15 lpm. From Fig. 8c, d, the experimental and RMS predicted NO<sub>x</sub> association was perfect ( $R^2$  was seen as 0.982). An analogous recurrence was discerned with all test run conditions.

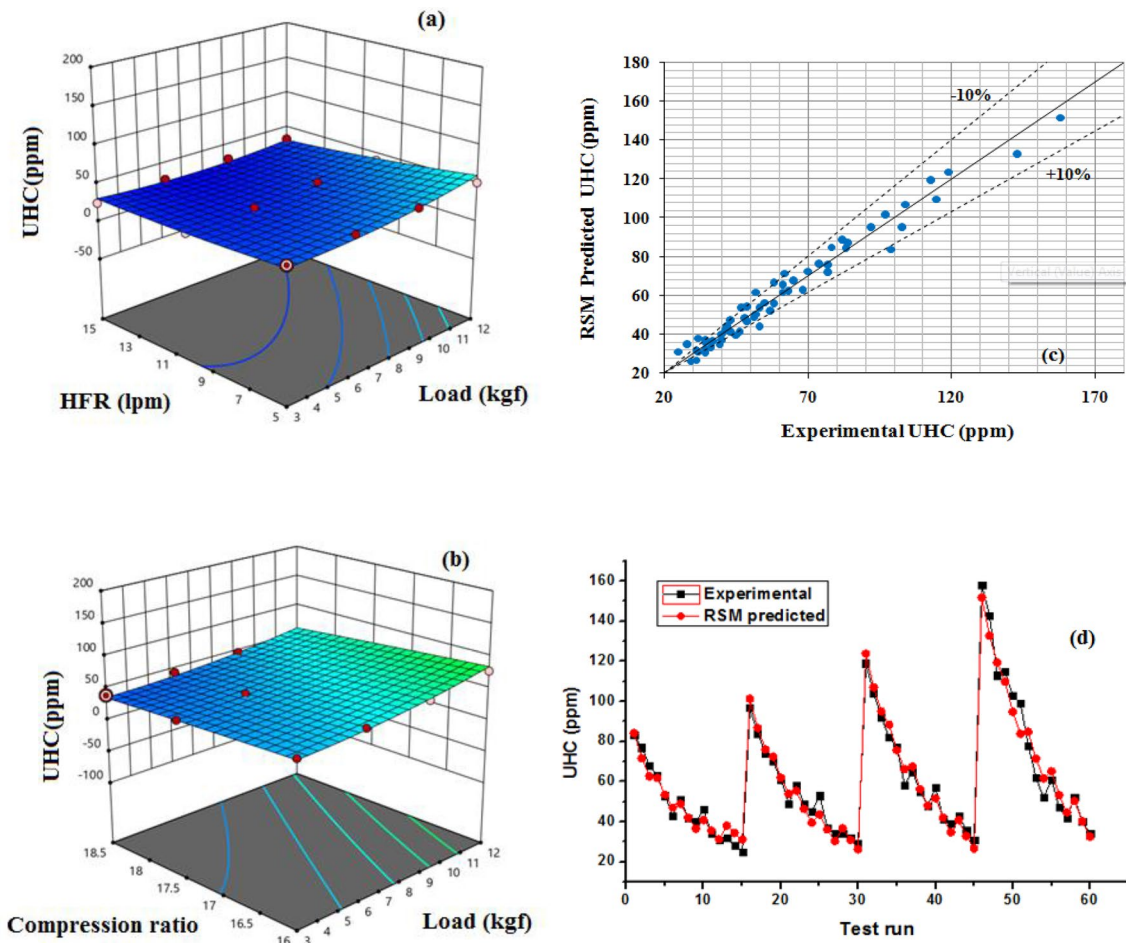


Fig.7 a–c Response surfaces of UHC b Experimental against RSM predicted UHC d UHC at different test runs

$$\begin{aligned}
 \text{NO}_x(\text{ppm}) = & 759.27 + (93.72 \times \text{FB}) + (59.94 \times \text{CR}) + (252.27 \times \text{Load}) + (159.63 \times \text{HFR}) \\
 & - (20.49 \times \text{FB} \times \text{CR}) - (7.56 \times \text{FB} \times \text{Load}) + (0.0000 \times \text{FB} \times \text{HFR}) - (10.35 \times \text{CR} \times \text{Load}) \\
 & + (26.55 \times \text{CR} \times \text{HFR}) + (23.09 \times \text{Load} \times \text{HFR}) + (0.0000 \times \text{FB}^2) + (21.58 \times \text{CR}^2) - (56.21 \times \text{Load}^2) + (14.62 \times \text{HFR}^2)
 \end{aligned} \tag{16}$$

#### 4.3.4 Smoke opacity

Figure 9a, b show the change in smoke opacity against compression ratio, load, and hydrogen flow rates. The smoke opacity was decreased with an increase in hydrogen quantity on account of elevated combustion which was because of the burning of the entire fuel. Besides, the smoke opacity was reduced with an increase in compression ratio because

of better combustion efficacy [24]. Further, at elevated loads, the smoke opacity was noticed higher. The minimum smoke opacity was attained at CR 18.5, HFR of 15 lpm, and a load condition of 3 kgf. Figure 9c, d presents the experimental and RSM predicted smoke opacity. It can be observed that the correlation between experimental and RSM predicted results were correct and the correlation coefficient ( $R^2$ ) was noticed as 0.969.

$$\begin{aligned}
 \text{Smoke}(\%) = & 12.03 - (2.83 \times \text{FB}) - (1.18 \times \text{CR}) + (9.33 \times \text{Load}) - (3.74 \times \text{HFR}) + (0.1007 \times \text{FB} \times \text{CR}) \\
 & + (0.4418 \times \text{FB} \times \text{Load}) + (0.0000 \times \text{FB} \times \text{HFR}) - (0.0714 \text{CR} \times \text{Load}) + (0.7466 \times \text{CR} \times \text{HFR}) \\
 & - (3.95 \times \text{Load} \times \text{HFR}) + (0.0000 \times \text{FB}^2) - (0.1405 \times \text{CR}^2) + (2.93 \times \text{Load}^2) + (0.4350 \times \text{HFR}^2)
 \end{aligned} \tag{17}$$

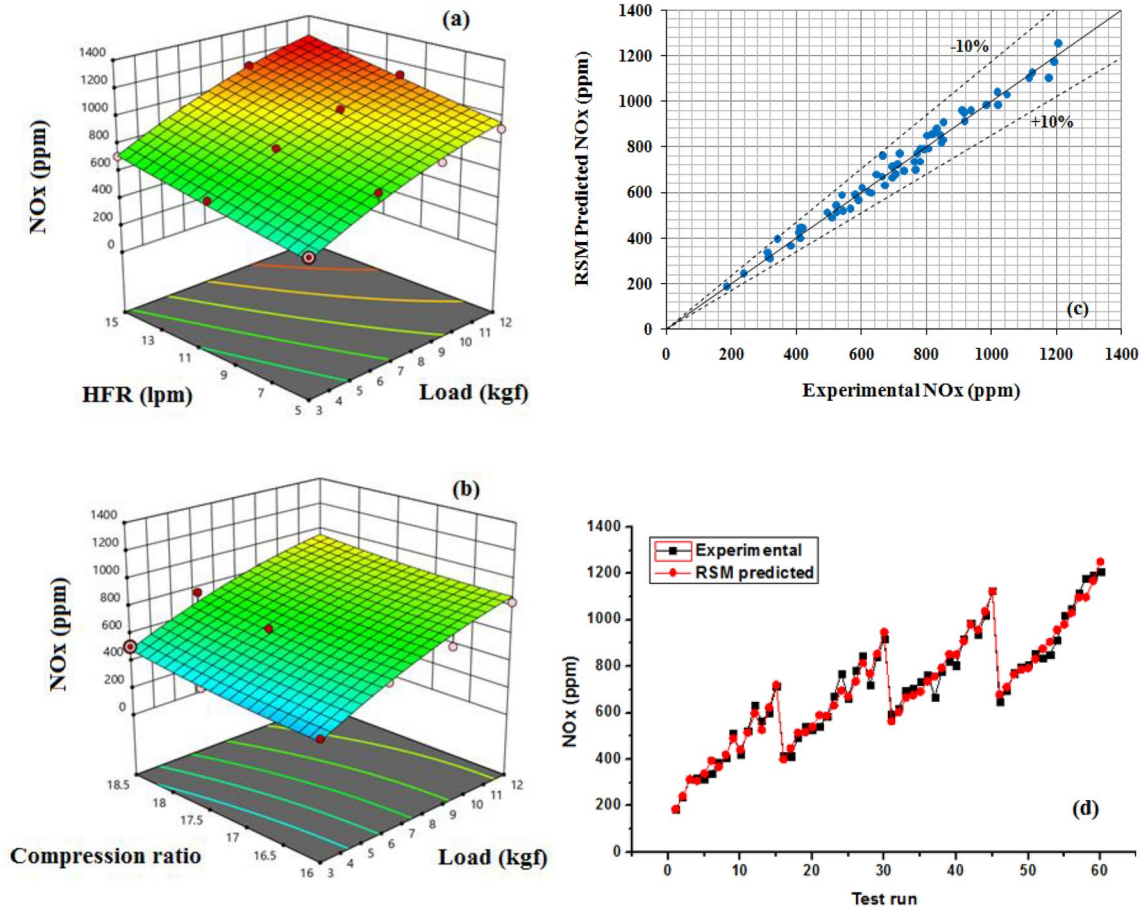


Fig.8 a, b Response surfaces of NO<sub>x</sub> c Experimental against RSM predicted NO<sub>x</sub> d NO<sub>x</sub> at different test runs

### 4.4 Vibration characteristics

#### 4.4.1 RMS velocity

Figure 10a, b describe the surface response variation of RMS velocity adjacent to compression ratio, load, and hydrogen flow rates. The notice made from Fig. 10a, b that the RMS velocity of hydrogen-enriched B20 was decreased. The motive for the decrement in RMS velocity was owing to superior combustion efficacy resulting in remarkable

augment in in-cylinder pressure. This improved cylinder pressure was as a result of the higher diffusion rate and a huge quantity of hydrogen accompany with fuel. Further, the RMS velocity was amplified towards a higher compression ratio due to fluctuation in-cylinder pressure [17]. RMS velocity at CR 16, HFR of 15 lpm, and at a load condition of 3 kgf was acquired minimum as 0.352 m/s. Figure 10c, d presents the experimental and RSM predicted smoke opacity. The correlation between experimental RMS velocity and RSM predicted RMS velocity was perfect and the R<sup>2</sup> was perceived as 0.961.

$$\begin{aligned}
 \text{RMS velocity}(m/s) = & 0.4225 - (0.0585 \times FB) + (0.0306 \times CR) + (0.0389 \times Load) - (0.0348 \times HFR) \\
 & + (0.0002 \times FB \times CR) + (0.0047 \times FB \times Load) + (0.0000 \times FB \times HFR) + (0.0002 \times CR \times Load) \\
 & - (0.0046 \times CR \times HFR) + (0.0042 \times Load \times HFR) + (0.0000 \times FB^2) \\
 & - (0.0002 \times CR^2) + (0.0327 \times Load^2) + (0.0095 \times HFR^2)
 \end{aligned} \tag{18}$$

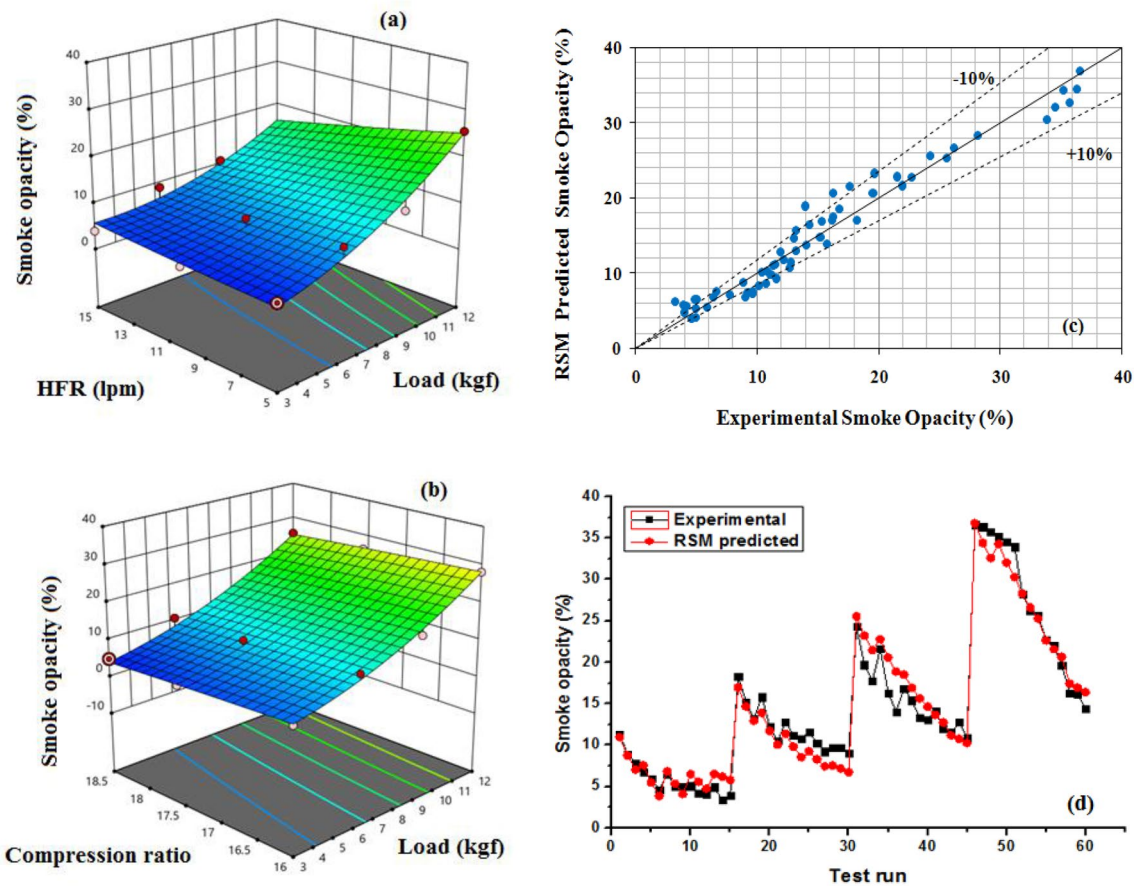


**Fig.9** a, b Response surfaces of smoke opacity c Experimental against RSM predicted smoke opacity d smoke opacity at different test runs

### 5 Conclusions

In this study, the NSOME blend (B20) and hydrogen was used as an alternative dual fuel source for assessing the performance, combustion, emission, and vibration parameters. The outcomes were summarized as follows.

The improvement in BTE and BSFC of B20 was inferior to ordinary diesel while it was improved significantly upon hydrogen supplement. An outstanding augmentation in combustion parameters (CP and NHRR) was also observed in dual fuel mode. Further, the greenhouse emissions (CO, UHC, and smoke were) with dual fuel has greatly reduced

apart from NO<sub>x</sub>. Finally, the RMS velocity (vibration) was inferior to dual fuel operations. Increase in CR has revealed the positive impact on performance, combustion, and emission (except NO<sub>x</sub>) parameters apart from vibrations.

RSM predicted and experimental outcomes were revealed in a finer connection. The correlation coefficient (R<sup>2</sup>) of all the parameters was noticed above 0.95 which signifies the superlative fit. The most extreme deviation of each parameter is within 10%. NSOME blend (B20) with hydrogen can be adopted as trusted alternative dual fuel in VCR engine without further changes of the engine. Further studies can be performed for the validation of combustion parameters

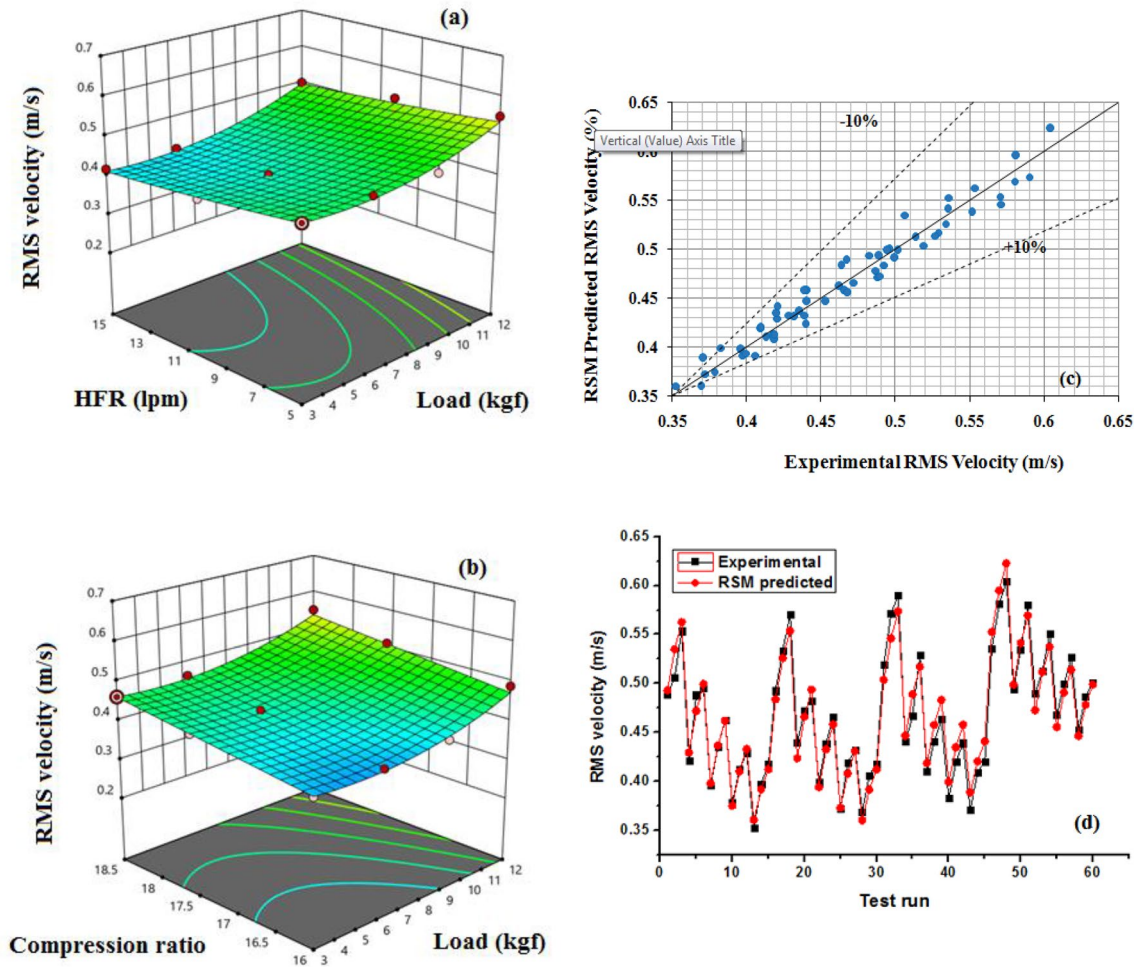


**Fig.10** a–c Response surfaces of RMS velocity **b** Experimental against RSM predicted RMS velocity **d** RMS velocity at different test runs

using computational fluid dynamics (CFD). Besides, the influence of nanoparticle additives in B20 could be studied for the reduction of NO<sub>x</sub> emission which is the foremost challenge in diesel engines.

### Compliance with ethical standards

**Conflict of interest** On behalf of all authors, the corresponding author states that there is no conflict of interest.

### Appendix

See Table 5.

**Table 5** input and output data set

Load (kgf)	Hydrogen flow rate (lpm)	Fuel blend (%)	CR	BTE (%)	BSFC (kg/kWhr)	CP (bar)	NHRR (J/deg)	CO (%)	UHC (ppm)	NOx (ppm)	Smoke (%)	RMS Velocity (m/s)
3	0	20	16	10.76615	0.80176	41.4	38.82	0.002	63	318	6.73	0.4209
3	5	20	16	11.09971	0.79533	46.16	46.51	0.004	51	386	6.46	0.3962
3	10	20	16	11.18832	0.78124	48.73	48.6	0.003	46	421	5.06	0.3783
3	15	20	16	11.24048	0.77019	51.04	49.51	0.002	32	566	4.93	0.3526
6	0	20	18.5	19.20028	0.45406	56.09	58.99	0.009	49	540	10.47	0.482764
6	5	20	16	18.17339	0.46806	50.88	54.75	0.012	58	584	12.82	0.39955
6	10	20	18.5	20.01398	0.42537	55.8	60.87	0.006	34	846	9.22	0.43229
6	15	20	18.5	20.49904	0.41551	57.38	61.57	0.003	29	919	9.06	0.418265
9	0	20	18.5	23.48958	0.36086	57.99	64.88	0.018	58	765	14.01	0.528749
9	5	20	16	22.88237	0.36155	52.83	59.43	0.018	65	669	16.85	0.4098
9	10	20	16	23.08137	0.35903	53.59	60.72	0.015	57	805	13.08	0.38279
9	15	20	18.5	25.15695	0.33522	59.14	65.87	0.007	31	1125	10.85	0.420558
12	0	20	18.5	24.61946	0.34757	59.7	62.72	0.047	99	854	33.91	0.58018
12	5	20	16	24.53794	0.35174	53.25	61.69	0.032	78	835	28.21	0.48959
12	10	20	18.5	26.09169	0.31268	61.734	66.11	0.013	42	1116	19.57	0.52689
12	15	20	18.5	26.8645	0.30495	62.88	68.81	0.008	34	1209	14.37	0.50123

## References

1. Sakthivel R, Ramesh K, Purnachandran R, Shameer PM (2018) A review on the properties, performance and emission aspects of the third generation biodiesels. *Renew Sustain Energy Rev* 82:2970–2992
2. Jaikumar S, Bhatti SK, Srinivas V (2019) Experimental investigations on performance, combustion, and emission characteristics of niger (*Guizotia abyssinica*) seed oil methyl ester blends with diesel at different compression ratios. *Arab J Sci Eng* 44:5263–5273
3. Bruno Alessandro D, Bidini G, Zampilli M, Laranci P, Bartocci P, Fantozzi F (2016) Straight and waste vegetable oil in engines: review and experimental measurement of emissions, fuel consumption and injector fouling on a turbocharged commercial engine. *Fuel* 182:198–209
4. Samuel OD, Okwu MO, Verma TN, Amosun ST, Afolalu SA (2019) Production of fatty acid ethyl esters from rubber seed oil in hydrodynamic cavitation reactor: study of reaction parameters and some fuel properties. *Ind Crop Product* 141(1):11658
5. Shrivastava P, Verma TN, Samuel OD, Pugazhendhi A (2020) An experimental investigation on engine characteristics, cost and energy analysis of CI engine fuelled with Roselle. *Karanja Biodiesel Blends Fuel* 275:117891
6. Senthur PS, Ashokan MA, Rahul R, Steff F, Sreelekh MK (2017) Performance, combustion and emission characteristics of diesel engine fueled with waste cooking oil bio-diesel/diesel blends with additives. *Energy* 122:638–648
7. Harveer SP, Kumar N, Alhaasan Y (2015) Performance and emission characteristics of an agriculture diesel engine fuelled with blends of sal methyl ester and diesel. *Energy Convers Manag* 90:146–153
8. Ahmet U (2018) Combustion, performance and emission characteristics of a DI diesel engine fueled with mustard oil biodiesel fuel blends at different engine loads. *Fuel* 212:256–267
9. Mohammad HO, Mohammed S (2016) Performance of CI engine operating with hydrogen supplement co-combustion with jojoba methyl ester. *Int J Hydrogen Energy* 41:10255–10264
10. Mohanad A, Radu C, Viorel B, Georges D, Pierre P (2017) Investigation on the mixture formation, combustion characteristics and performance of a Diesel engine fueled with Diesel, Biodiesel (B20) and hydrogen addition". *Int J Hydrogen Energy* 42:16793–16807
11. Rahman MA, Ruhul AM, Aziz MA, Ahmed R (2017) Experimental exploration of hydrogen enrichment in a dual fuel CI engine with exhaust gas recirculation. *Int J Hydrogen Energy* 42:5400–5409
12. Jaikumar S, Bhatti SK, Srinivas V (2019) Experimental explorations of dual fuel CI engine operating with *Guizotia abyssinica* methyl ester–diesel blend (B20) and hydrogen at different compression ratios. *Arab J Sci Eng*. pp 1–11
13. Alpaslan A, Yuksel B, Ileri E, Karaoglan AD (2015) Response surface methodology based optimization of diesel–n-butanol–cotton oil ternary blend ratios to improve engine performance and exhaust emission characteristics. *Energy Convers Manage* 90:383–394
14. Prasada Rao K, Appa Rao BV (2016) Parametric optimization for performance and emissions of an IDI engine with Mahua biodiesel. *Egypt J Pet*. pp 1–11
15. Bharadwaz YD, Rao BG, Rao VD, Anusha C (2016) Improvement of biodiesel methanol blends performance in a variable compression ratio engine using response surface methodology. *Alexandria Engineering Journal* 55(2):1201–1209
16. Molina S, Guardiola C, Martin J, Garcia-Sarmiento D (2014) Development of a control-oriented model to optimize fuel consumption and NOx emissions in a DI Diesel engine. *Appl. Energy* 119:405–416
17. Jaikumar S, Bhatti SK, Srinivas V, Rajasekhar M (2020) Vibration and noise characteristics of CI engine fueled with Niger seed oil methyl ester blends and hydrogen. *Int J Eng Sci Technol* 17:1529–1536
18. Krishnamoorthi M, Malayalamurthi R, Shameer P (2018) RSM based optimization of performance and emission characteristics of DI compression ignition engine fuelled with diesel/aegle marmelos oil/diethyl ether blends at varying compression ratio, injection pressure and injection timing. *Fuel* 221:283–297
19. Saravanan N, Nagarajan G (2008) An experimental investigation of hydrogen-enriched air induction in a diesel engine system. *Int J Hydrog Energy* 33:1769–1775
20. Pavlos D, Taku T (2017) A review of hydrogen as a compression ignition engine fuel. *Int J Hydrog Energy* 42:24470–24486
21. Yilmaz IT, Demir A, Gumus M (2017) Effects of hydrogen enrichment on combustion characteristics of a CI engine. *Int J Hydrog Energy* 42:10536–10546
22. Tadveer SH, Avinash KA (2016) Effect of varying compression ratio on combustion, performance, and emissions of hydrogen enriched compressed natural gas fuelled engine. *J Nat Gas Sci Eng* 31:819–828
23. Mohanad A, Radu C, Viorel B, Georges D, Pierre P (2017) Investigation on the mixture formation, combustion characteristics and performance of a diesel engine fueled with diesel, biodiesel (B20) and hydrogen addition. *Int J Hydrog Energy* 42:16793–16807
24. Tangoz S, Akansu SO, Kahraman N, Malkoc Y (2016) Effects of compression ratio on performance and emission of a modified diesel engine fueled by HCNG. *Int J Hydrog Energy* 40:15374–15380
25. Madhujit D, Abhishek P, Durbadal D, Sastry GRK, Raj SP, Bose PK (2015) An experimental investigation of performance emission trade off characteristics of a CI engine using hydrogen as dual fuel. *Energy* 85:569–585

**Publisher's Note** Springer Nature remains neutral with regard to jurisdictional claims in published maps and institutional affiliations.